ACS APPLIED MATERIALS & INTERFACES

Research Article

www.acsami.org

Solution-Processable BODIPY-Based Small Molecules for Semiconducting Microfibers in Organic Thin-Film Transistors

Mehmet Ozdemir,[†,#] Donghee Choi,[‡,#] Guhyun Kwon,[‡] Yunus Zorlu,[§] Bunyemin Cosut,[§] Hyekyoung Kim,[‡] Antonio Facchetti,[*,∥,⊥] Choongik Kim,[*,‡] and Hakan Usta[*,†]

[†]Department of Materials Science and Nanotechnology Engineering, Abdullah Gül University, Kayseri 38080, Turkey

[‡]Department of Chemical and Biomolecular Engineering, Sogang University, Mapo-gu, Seoul 121-742, Korea

[§]Department of Chemistry, Gebze Technical University, Gebze 41400, Turkey

[∥]Polyera Corporation, 8045 Lamon Avenue, Skokie, Illinios 60077, United States

[⊥]Center of Excellence for Advanced Materials Research (CEAMR), King Abdulaziz University, Jeddah 21589, Saudi Arabia

Supporting Information

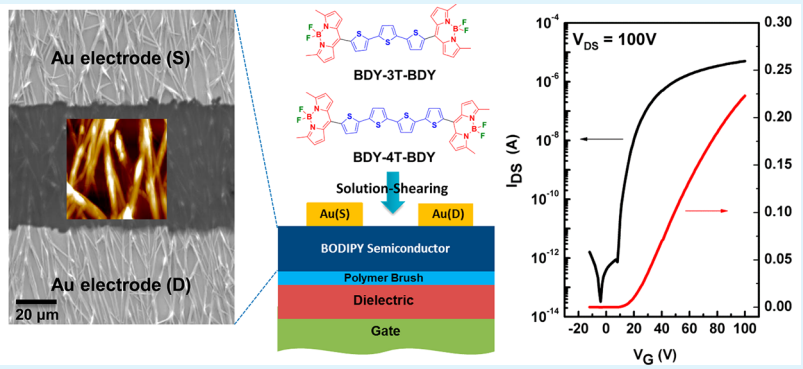

ABSTRACT: Electron-deficient π-conjugated small molecules can function as electron-transporting semiconductors in various optoelectronic applications. Despite their unique structural, optical, and electronic properties, the development of BODIPY-based organic semiconductors has lagged behind that of other π-deficient units. Here, we report the design and synthesis of two novel solution-proccessable BODIPY-based small molecules (**BDY-3T-BDY** and **BDY-4T-BDY**) for organic thin-film transistors (OTFTs). The new semiconductors were fully characterized by $^{1}H/^{13}C$ NMR, mass spectrometry, cyclic voltammetry, UV−vis spectroscopy, photoluminescence, differential scanning calorimetry, and thermogravimetric analysis. The single-crystal X-ray diffraction (XRD) characterization of a key intermediate reveals crucial structural properties. Solution-sheared top-contact/bottom-gate OTFTs exhibited electron mobilities up to 0.01 $cm^2/V{\cdot}s$ and current on/off ratios of $>10^8$. Film microstructural and morphological characterizations indicate the formation of relatively long (~0.1 mm) and micrometer-sized (1−2 μm) crystalline fibers for **BDY-4T-BDY**-based films along the shearing direction. Fiber-alignment-induced charge-transport anisotropy ($\mu_{\parallel}/\mu_{\perp} \approx 10$) was observed, and higher mobilities were achieved when the microfibers were aligned along the conduction channel, which allows for efficient long-range charge-transport between source and drain electrodes. These OTFT performances are the highest reported to date for a BODIPY-based molecular semiconductor, and demonstrate that BODIPY is a promising building block for enabling solution-processed, electron-transporting semiconductor films.

KEYWORDS: *organic thin-film transistor, n-channel semiconductor, BODIPY, small molecule-based microfiber*

1. INTRODUCTION

4,4-Difluoro-4-bora-3*a*,4*a*-diaza-*s*-indacene (BODIPY)-based π-conjugated structures have been widely studied in the past few decades for the realization of highly fluorescent functional dyes.[1] Following the initial synthesis of the BODIPY core in the late 1960s, numerous rationally designed BODIPY-based small molecules and macromolecules have been developed, and they were investigated for a broad range of applications including fluorescent switches, biochemical labeling, chemosensors, and electroluminescent devices.[2−4] Indeed, BODIPY-based dyes exhibit excellent thermal/photochemical stability, good solubility, intense absorption/emission profiles, high photoluminescence quantum yield, and small Stokes shifts.[5,6]

In addition, the BODIPY system's optical and electronic characteristics are tunable via facile synthetic modifications on the boron-dipyrromethene core.[7,8] Despite all of these advantages, to date very few BODIPY-based molecular and polymeric semiconductors have been studied in optoelec-

Received: March 5, 2016
Accepted: May 16, 2016
Published: May 16, 2016

DOI: 10.1021/acsami.6b02788
ACS Appl. Mater. Interfaces 2016, 8, 14077−14087

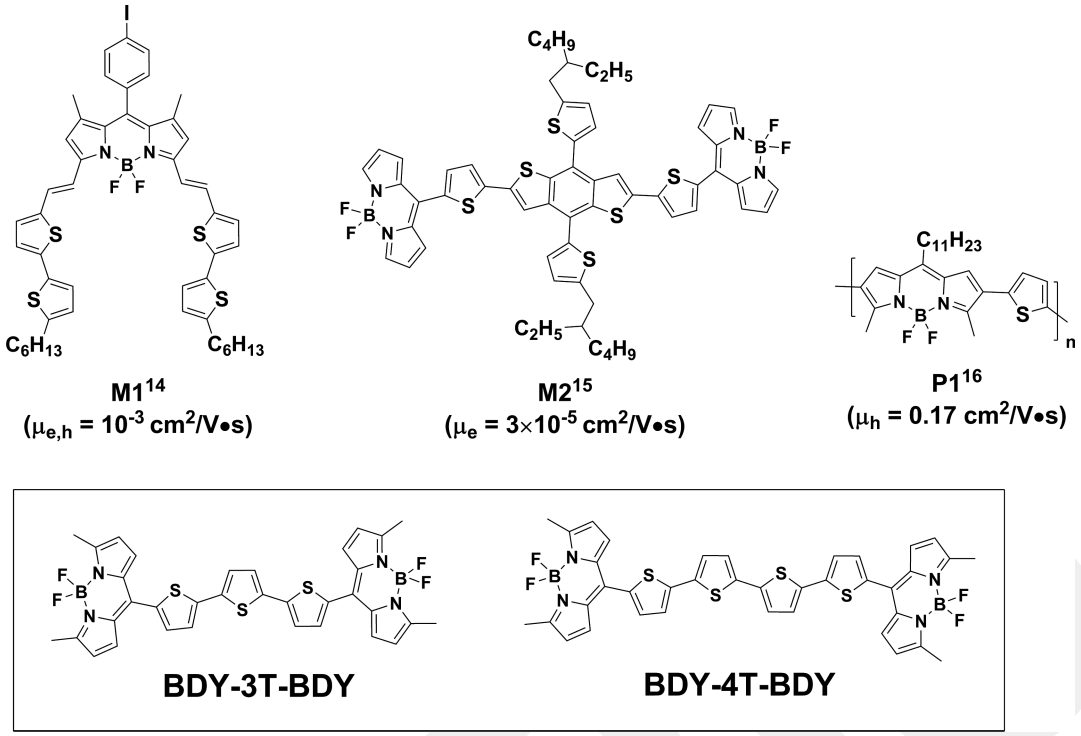

Figure 1. Chemical structures of previously reported BODIPY-based semiconductors **M1**,[14] **M2**,[15] and **P1**,[16] and **BDY-3T-BDY** and **BDY-4T-BDY** developed in this study.

tronics,[9−13] and more specifically in organic thin-film transistors (OTFTs), with the most promising ones (**M1** and **M2** in Figure 1) exhibiting relatively low OTFT charge carrier mobilities of ∼10^{-5}−10^{-3} $cm^2/V{\cdot}s$.[14,15] To this end, we have recently developed a series of BODIPY-thiophene copolymers, in which the charge carrier mobility was enhanced to μ_h = 0.17 $cm^2/V{\cdot}s$ (>10 000×), remaining the highest mobility BODIPY-based polymer semiconductor (**P1** in Figure 1).[16] Because such high mobilities were accessible only for BODIPY-based π-conjugated polymeric backbones, the interesting question is whether substantial mobilities are possible for BODIPY-based molecular semiconductors. From a materials perspective, small molecules are advantageous over polymers because of synthetic reproducibility, structural versatility, ease of purification, monodispersity, and high degree of crystallinity.[17−22] Thus, the rational engineering of molecular architectures embedding properly designed BODIPY units is very crucial to enhance charge-transport as well as to better understand of the properties of BODIPY-based systems. Realization of good charge-transport with BODIPY-based molecular systems is expected to greatly advance technologies where both charge-transport and photophysical processes take place such as in organic photovoltaics (OPVs), organic light-emitting diodes (OLEDs), and organic light-emitting transistors (OLETs).[23−28]

Here, we report the design and synthesis of two new molecular semiconductors **BDY-3T-BDY** and **BDY-4T-BDY** (Figure 1) based on an acceptor−donor−acceptor (A−D−A) molecular architecture, in which BODIPY and terthiophene (3T)/quaterthiophene (4T) units are used as acceptor and donor units, respectively. BODIPYs are connected to the α,ω-oligothiophene cores through their *meso*-positions to achieve linear and symmetrical molecular architectures featuring π-conjugation and optimized molecular energetics. It is noteworthy that the approach of employing π-electron deficient units at the molecular termini of a π-donor has been successfully utilized to enable numerous *n*-channel semiconductors.[29,30] Therefore, in the semiconductor design, we envision that BODIPY may be an ideal acceptor end unit because it has strong electron-withdrawing characteristics, and it may provide negative inductive (−I) and mesomeric (−M) effects. This approach should facilitate the delocalization and stabilization of charge carriers (i.e., electrons). The new semiconductors are designed without any lipophilic substitution on the 3,4′-thiophene and 1,7-BODIPY positions to minimize intramolecular torsions and maximize intermolecular interactions. Furthermore, the BODIPY unit exhibits strong dipoles (μ = 3.38 D) oriented toward the 4,4′-fluorine substituents, which could facilitate dipolar intermolecular interactions and result in ordered thin-film phases. This dipole is also expected to enhance the solubility of the current semiconductors via dipolar interactions with the solvent molecules. In addition, the presence of fluorine atoms may induce nonbonding intermolecular interactions (e.g., −F···S− and −F···N−) to enhance thin-film ordering. The new semiconductors were characterized by $^1H/^{13}C$ NMR, mass spectrometry, cyclic voltammetry, UV−vis spectroscopy, differential scanning calorimetry, and thermogravimetric analysis. The single-crystal X-ray diffraction (XRD) characterization of a key intermediate reveals crucial structural properties. Top-contact/bottom-gate OTFT devices were fabricated by physical vapor deposition or solution shearing the semiconductors, and the resulting devices exhibited *n*-channel charge-transport with electron mobilities of up to 0.01 $cm^2/V{\cdot}s$ and current on/off ratio of >10^8, which is currently the highest reported to date for BODIPY-based molecular semiconductors. Although these performances are lower than those of the state-of-the-art solution-processed OTFT devices, it is regarded as an important step toward the

DOI: 10.1021/acsami.6b02788
ACS Appl. Mater. Interfaces 2016, 8, 14077−14087

realization of high performance BODIPY-based semiconductor films.

2. EXPERIMENTAL SECTION

Materials and Methods. All reagents were purchased from commercial sources and used without further purification unless otherwise noted. Conventional Schlenk techniques were used, and reactions were carried out under N_2 unless otherwise noted. NMR spectra were recorded on a Bruker 400 spectrometer (^{1}H, 400 MHz; ^{13}C, 100 MHz). Elemental analyses were performed on a LecoTruspec Micro model instrument. MALDI-TOF was performed on a Bruker Microflex LT MALDI-TOF-MS instrument. Thermogravimetric analysis (TGA) and differential scanning calorimetry (DSC) measurements were performed on PerkinElmer Diamond model instruments under nitrogen at a heating rate of 10 °C/min. UV−vis absorption measurements were performed on a Shimadzu, UV-1800 UV−vis spectrophotometer. Fluorescence emission spectra were recorded on a Varian Eclipse spectrofluorometer using 1 cm path length cuvettes at room temperature. The fluorescence quantum yield values were determined in toluene or THF by comparing with the fluorescence of Rhodamine 6G as the standard (Φ_F = 0.76 in water). Electrochemistry was performed on a C3 Cell Stand electrochemical station equipped with BAS Epsilon software (Bioanalytical Systems, Inc., Lafayette, IN). Prior to the synthesis, the optimization of the molecular geometries and total energy calculations were carried out using density functional theory (DFT) at the B3LYP/6-31G** level with Gaussian 09.[31]

Crystal Structure Determination. The intensity data for **BDY-1** were collected on a Bruker APEX II QUAZAR three-circle diffractometer using monochromatized Mo K_α X-radiation (λ = 0.71073 Å). Indexing was performed using APEX2.[32] Data integration and reduction were carried out with SAINT.[33] Absorption correction was performed by multiscan method implemented in SADABS.[34] The structure was solved and refined using the Bruker SHELXTL Software Package.[35] All non-hydrogen atoms were refined anisotropically using all reflections with $I > 2\sigma(I)$. The C-bound H atoms were positioned geometrically and refined using a riding mode. Crystallographic data and refinement details of the data collection for **BDY-1** are summarized in Table S1. CCDC 1435038 (for **BDY-1**) contains the supplementary crystallographic data for this paper. These data can be obtained free of charge from The Cambridge Crystallographic Data Centre via www.ccdc.cam.ac.uk/data_request/cif. The final geometrical calculations and the molecular drawings for **BDY-1** were carried out with Platon (version 1.17)[36] and Mercury CSD (version 3.5.1)[37] programs.

*Synthesis of 5-Bromo-2-thiophenecarbaldehyde (**1**).* *N*-Bromosuccinimide (8.7 g, 49.04 mmol) was slowly added to a solution of 2-thiophenecarboxaldehyde (5.0 g, 44.6 mol) in anhydrous $CHCl_3$ (100 mL). The reaction mixture was stirred for 14 h at room temperature. The mixture then was extracted with $CHCl_3$, and the organic phase was washed with deionized water, dried over Na_2SO_4, filtered, and evaporated to dryness to give the crude product. Purification by column chromatography on silica gel using $CHCl_3$ as the eluent affords the pure product as a colorless oil (8.3 g, 97.5%). ^{1}H NMR (400 MHz, $CDCl_3$): δ 7.20 (d, H, J = 4.0 Hz), 7.53 (d, H, J = 8.0 Hz), 9.79 (s, H).

*Synthesis of 8-(2-Bromothien-5-yl)-3,5-dimethyl-4,4-difluoro-4-bora-3a,4a-diaza-s-indacene (**BDY-1**).* To a solution of 5-bromo-2-thiophenecarbaldehyde (**1**) (0.70 g, 3.66 mmol) and 2-methylpyrrole (**2**) (0.67 g, 8.28 mmol) in degassed CH_2Cl_2 (220 mL) was added trifluoroacetic acid (TFA) (2 drops) under nitrogen, and the mixture was stirred at ambient temperature overnight. Next, 2,3-dichloro-5,6-dicyano-1,4-benzoquinone (DDQ) (0.83 g, 3.66 mmol) was added, and the reaction mixture was stirred for additional 2.5 h. Finally, *N*,*N*-diisopropylethylamine (i-Pr)$_2$EtN (2.60 g, 20.05 mmol) and boron trifluoride diethyl etherate (BF_3·Et_2O) (1.81 g, 12.7 mmol) were added, and the reaction mixture was stirred for 2 h. The reaction mixture was poured into water and extracted with CH_2Cl_2. The organic phase was dried over Na_2SO_4, filtered, and evaporated to dryness to give a crude product, which was purified by column chromatography on silica gel using CH_2Cl_2:hexanes (2:1) as the eluent. The pure product was obtained as a crystalline red solid (0.57 g, 41% yield). mp 132−133 °C. ^{1}H NMR (400 MHz, $CDCl_3$): δ 2.68 (s, 6H), 6.32 (d, 2H, J = 4.0 Hz), 7.05 (d, 2H, J = 4.0 Hz), 7.19 (m, 2H). ^{13}C NMR (100 MHz, $CDCl_3$): 15.0, 116.9, 119.7, 130.1, 130.6, 131.7, 133.2, 133.9, 136.1, 158.2.

*Synthesis of 5,5″-Bis(3,5-dimethylBODIPY-8-yl)-2,2′:5′,2″-terthiophene (**BDY-3T-BDY**).* The reagents **BDY-1** (0.48 g, 1.25 mmol), 2,5-bis(trimethylstannyl)thiophene (**3**) (0.24 g, 0.60 mmol), and Pd(PPh$_3$)$_2$Cl$_2$ (0.013 g, 17.8 μmol) in anhydrous toluene (30 mL) were heated at 110 °C under nitrogen for 48 h. The reaction mixture then was cooled to room temperature and evaporated to dryness. The crude product was filtered by using methanol, and then washed with methanol to give a dark crude solid, which was purified by column chromatography on silica gel with $CHCl_3$:hexanes (1:1) as the eluent to give the final product as a dark red solid (0.20 g, 49% yield). $T_{decomposition}$ > 250 °C. ^{1}H NMR (400 MHz, $CDCl_3$): δ 2.68 (s, 6H), 6.35 (m, 2H), 7.15 (m, 2H), 7.22−7.42 (m, 3H). ^{13}C NMR (100 MHz, $CDCl_3$): 15.0, 119.5, 119.7, 124.4, 124.5, 125.0, 125.2, 125.7, 130.1, 132.6, 132.8, 133.8, 134.7, 140.4, 157.6, 157.7, 158.1. MS(MALDI-TOF) m/z (M^+): calcd for $C_{34}H_{26}B_2F_4N_4S_3$, 684.14; found, 684.96 $[M + H]^+$, 664.88 $[M - F]^+$, 602.78 $[M - 4\times CH_3 - F]^+$, 583.70 $[M - 4\times CH_3 - 2\times F]^+$. Anal. Calcd for $C_{34}H_{26}B_2F_4N_4S_3$: C, 59.67; H, 3.83; N, 8.19. Found: C, 59.83; H, 4.07; N, 7.89.

*Synthesis of 5,5‴-Bis(3,5-dimethylBODIPY-8-yl)-2,2′:5′,2″:5″,2‴-quaterthiophene (**BDY-4T-BDY**).* The reagents **BDY-1** (0.40 g, 1.05 mmol), 5,5′-bis(trimethylstannyl)-2−2′-thiophene (**4**) (0.24 g, 0.50 mmol), and Pd(PPh$_3$)$_2$Cl$_2$ (0.022 g, 0.03 mmol) in anhydrous toluene (30 mL) were heated at 110 °C under nitrogen for 48 h. The reaction mixture then was cooled to room temperature and evaporated to dryness. The crude product was filtered by using methanol, and then washed with methanol to give a dark crude solid. The crude product was purified by column chromatography on silica gel with CH_2Cl_2:hexanes (1:1) as the eluent to give final product as a dark red solid (0.17 g, 44% yield). $T_{decomposition}$ > 250 °C. ^{1}H NMR (400 MHz, $CDCl_3$): δ 2.67 (s, 6H), 6.35 (m, 2H), 7.15−7.42 (m, 6H). ^{13}C NMR (100 MHz, $CDCl_3$): 15.0, 119.6, 119.7, 124.4, 125.0, 125.2, 125.8, 130.1, 132.7, 132.8, 133.6, 133.8, 133.9, 134.7, 135.4, 137.0, 140.4, 141.5, 157.7, 158.0. MS(MALDI-TOF) m/z (M^+): calcd for $C_{38}H_{28}B_2F_4N_4S_4$, 766.13; found, 767.12 $[M + H]^+$, 748.03 $[M - F]^+$. Anal. Calcd for $C_{38}H_{28}B_2F_4N_4S_4$: C, 59.54; H, 3.68, N, 7.31. Found: C, 59.05; H, 3.84, N, 7.60.

Device Fabrication and Characterization. For the fabrication of top-contact/bottom-gate organic thin-film transistors (OTFTs), highly *n*-doped (100) silicon wafers (resistivity <0.005 Ω cm) with a 300 nm thermally grown oxide gate dielectric film were used as device substrates. The Si/SiO_2 substrates were washed via sonication in acetone for 10 min, followed by oxygen plasma for 5 min (18 W). The general recipes were employed for the treatment of gate dielectric layers including three self-assembled monolayers (octadecyltrimethoxysilane, OTMS; hexamethyldisilane, HMDS; phenyltrichlorosilane, PTS) and PS-brush.[15] Semiconducting layers (**BDY-3T-BDY** and **BDY-4T-BDY**) were formed via vacuum deposition or solution-shearing (SS). For vacuum deposition, OTMS, HMDS, and PTS substrates were used. Semiconducting layer was deposited under high vacuum (~2 × 10^{-5} Torr) at various substrate temperatures (T_D's) of 25, 50, and 80 °C. For solution-shearing process, PS-brush-treated substrates were employed. The solution-shearing process was performed in accordance with the reported procedure.[54] During the solution-shearing process, a few drops of semiconductor solution (~1 mg/mL) were cast onto a heated substrate (1 cm × 2 cm), and the substrate was covered with a dewetting OTS-modified top substrate. The top substrate was fixed with bar to the syringe pump and tilted at small angle (<10°). The dewetting top substrate was then translated by an electrically controlled syringe pump at a constant velocity relative to the bottom substrate, gradually uncovering the sandwiched solution, which quickly evaporated and left behind a polycrystalline thin-film seeding from the shearing substrate frontier. Solvent evaporation was controlled by different solution-shearing conditions such as deposition temperature (50−80% of the solvent boiling point) and different

DOI: 10.1021/acsami.6b02788
ACS Appl. Mater. Interfaces 2016, 8, 14077−14087

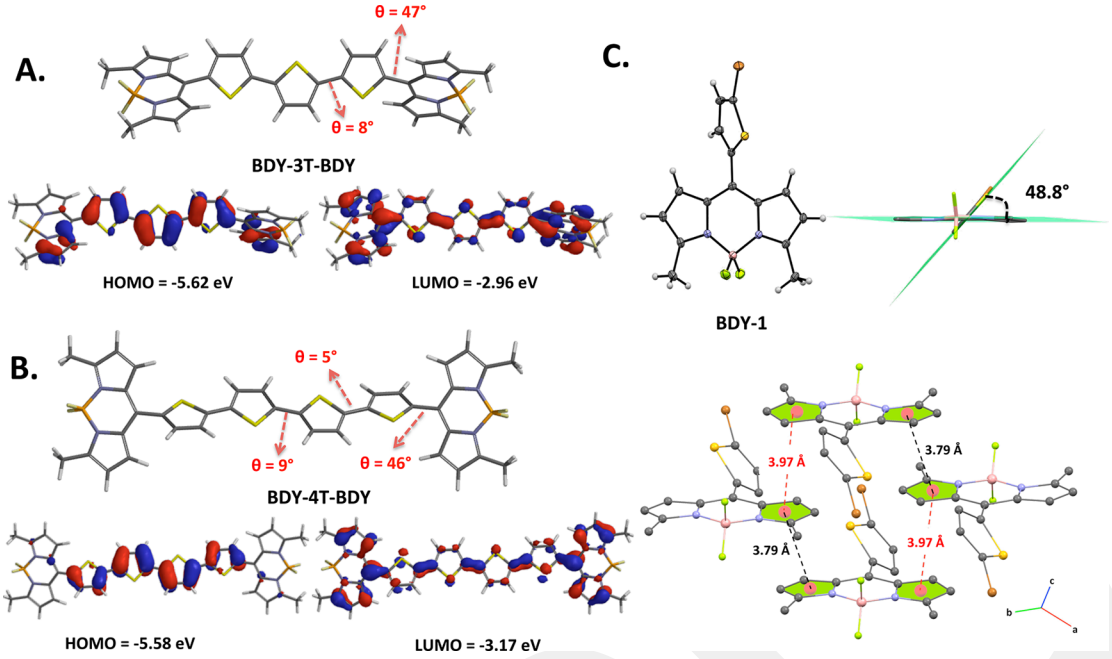

Figure 2. Optimized molecular geometries of **BDY-3T-BDY** (A) and **BDY-4T-BDY** (B) showing inter-ring torsional angles (θ), computed HOMO and LUMO energy levels, and molecular orbital topographical representations (DFT, B3LYP/6-31G**). (C) ORTEP drawings of the crystal structure of **BDY-1** (20% probability level), and the perspective view of inter-ring dihedral angle between boron-dipyrromethene and *meso*-thiophene planes, and $\pi-\pi$ stacking interactions between pyrrole units. (The gray, brown, blue, pink, yellow, and white colored atoms represent C, Br, N, B, F, and H, respectively.)

solution shearing speed (0.1−4 mm/min). The solution-sheared substrates were placed in a vacuum oven at 90 °C overnight to remove the residual solvent. The solution-shearing process was optimized with regards to solvent type, substrate temperature, and shearing speed. Film thicknesses were characterized by profilometer (DEKTAK-XT, Bruker) as 40−60 nm (vacuum deposited films) and 300−650 nm (solution-sheared films), respectively. Au layers (40 nm) were thermally evaporated through a shadow mask to define source and drain contacts with various channel lengths (L; 100 and 50 μm) and widths (W; 1000 and 500 μm).

The electronic characteristics of OTFTs were measured using a Keithley 4200-SCS in a vacuum probe station ($P < 10^{-5}$ Torr). Carrier mobilities (μ), threshold voltages (V_T), and I_{on}/I_{off} ratios were calculated in the saturation regime by the formula:

$$\mu_{sat} = (2I_{DS}L)/[WC_i(V_G - V_T)^2]$$

where I_{DS} is the source-drain current, L is the channel length, W is the channel width, C_i is the areal capacitance of the gate dielectric (C_i = 11.4 nF cm^{-2}), V_G is the gate voltage, and V_T is the threshold voltage. The reported values are the average of 10 different devices with the standard deviations of less than 5%. The microstructure and surface morphology of thin-films were analyzed by optical microscopy (HDC-SD044S, HDView), atomic force microscope (AFM, NX10, Park systems), X-ray diffraction (XRD, Smartlab, Rigaku), and scanning electron microscope (SEM, JSM-6010LA, JEOL).

3. RESULTS AND DISCUSSION

Computational Modeling, Synthesis, and Characterization. Prior to the synthesis, DFT calculations were performed at the B3LYP/6-31G** level of theory to evaluate molecular geometries and frontier molecular orbital energetics. As shown in Figure 2A and B, DFT calculations indicate that the oligothiophene cores of both **BDY-3T-BDY** (terthiophene) and **BDY-4T-BDY** (quaterthiophene) molecules are highly planar, featuring maximum inter-ring torsional angles of <10°. This result ensures an efficient π-orbital delocalization along the donor part. On the other hand, large inter-ring torsional angles (~46−49°) were calculated between the boron-dipyrromethene and the *meso*-thiophene units in both the intermediate compound **BDY-1** (Figure S2) and the final compounds **BDY-3T-BDY** and **BDY-4T-BDY** (Figure 2A and B). These relatively large torsions are confirmed by the single-crystal structure analysis of the subunit **BDY-1** (Figure 2C). Red crystals of **BDY-1** suitable for single-crystal analysis were obtained in suitable sizes by diffusion of methanol into a chloroform solution at room temperature. **BDY-1** crystallizes in the monoclinic space group $P2_1/c$, and the boron-dipyrromethene core (C_9BN_2) adopting a highly planar geometry with a maximum deviation from the least-squares plane of only 0.070(3) Å. The inter-ring torsional angle between the *meso*-thiophene group and the boron-dipyrromethene plane is 48.80°, which matches well with the computationally optimized geometries. This angle is small as compared to those of previously reported *meso*-aromatic substituted BODIPY small molecules (Figure S1, θ = 56−90°), which is probably due to the lack of β-pyrrole substituents and sterically less-encumbered nature of the five-membered thiophene ring.[38] Thus, our structural approach should offer a significant advantage to enhance charge-transport in the solid state when compared to the previously reported BODIPY-based semiconductors.[39] Comparable donor−acceptor dihedral angles were reported between thiophene and naphthalenediimide (NDI)/perylenediimide (PDI) units in several high-performance *n*-channel semiconductors.[40−42] The boron-dipyrromethene core in **BDY-1** exhibits slipped cofacial π-stacked packing motif with a favorable interplanar $\pi-\pi$ stacking distance of 3.79−3.97 Å through pyrrole rings (Figure 2C), again possibly favoring charge carrying properties in the solid state.

The MO computed HOMO/LUMO energies were found to be −5.62/−2.96 eV for **BDY-3T-BDY** and −5.58/−3.17 eV for

DOI: 10.1021/acsami.6b02788
ACS Appl. Mater. Interfaces 2016, 8, 14077−14087

Scheme 1. Synthesis of BDY-3T-BDY and BDY-4T-BDY

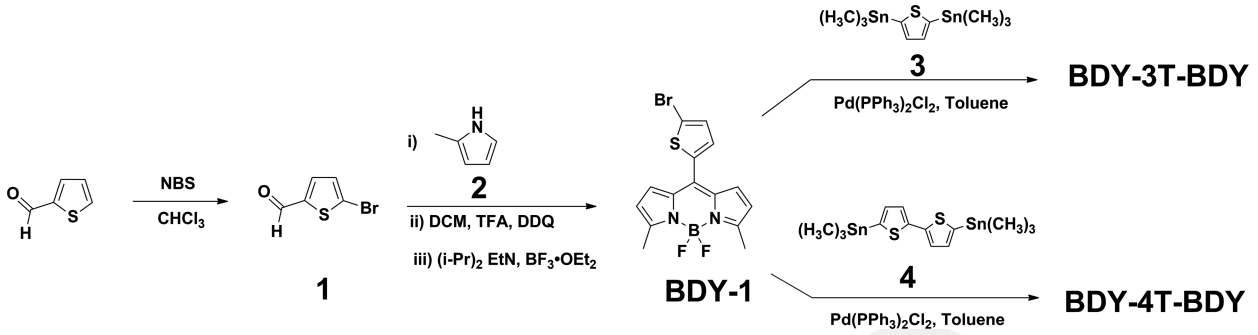

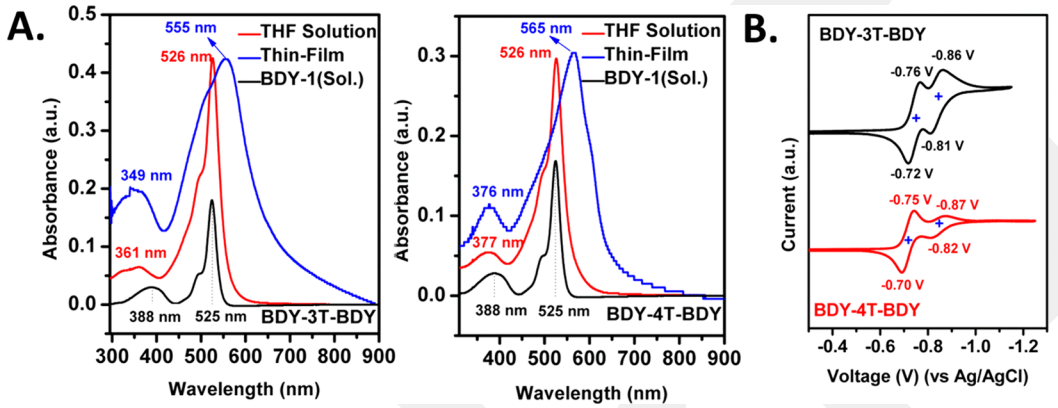

Figure 3. (A) Optical absorption spectra of **BDY-3T-BDY** and **BDY-4T-BDY** in THF solution and as thin-films. (B) Cyclic voltammograms of **BDY-3T-BDY** and **BDY-4T-BDY** in THF (0.1 M $Bu_4N^+PF_6^-$, scan rate = 50 mV s^{-1}).

BDY-4T-BDY, and molecular topology supports highly extended π-orbital delocalizations despite the severe torsions. Because the HOMO is more localized on the oligothiophene π-donor and the LUMO has larger electron density on the terminal BODIPY π-acceptor, HOMO → LUMO optical transitions may be dominated by partial charge transfers (vide infra). As compared to π-electron-rich terthiophene and quaterthiophene oligomers (Figure S2), MO computations demonstrate that the molecular energy levels of the new A−D−A molecules are found to be highly stabilized (ΔE_{LUMO} = −(1.2−1.3) eV and ΔE_{HOMO} = −(0.5−0.6) eV) as a result of the electron-deficiency of the BODIPY end units. The relatively large LUMO orbital stabilization, and its π-extended delocalization along the molecular backbone with significant spatial orbital distribution on the BODIPYs, are expected to facilitate *n*-channel transport in the current semiconductors. The LUMO energy levels are in the range of those calculated for previously reported *n*-channel semiconductors (−2.5 to −4.3 eV), indicating that the new molecules are most likely to exhibit electron-transporting characteristics.[43]

The synthetic routes to the new semiconductors are shown in Scheme 1. Because of the instability of unsubstituted dipyrromethene, BODIPY end-unit was synthesized with two methyl groups in the α-positions. The common intermediates **2**, **3**, and **4** were prepared according to literature procedures (Scheme S1). The boron-dipyrromethene intermediate **BDY-1** was prepared by first reacting 5-bromo-2-thiophenecarboxaldehyde (**1**) with 2-methyl pyrrole (**2**) in the presence of a catalytic amount of trifluoroacetic acid (TFA), which was subsequently oxidized with 2,3-dichloro-5,6-dicyano-1,4-benzoquinone (DDQ) and coordinated with trifluoroborane diethetate ($BF_3{\cdot}OEt_2$) in the presence of $(i\text{-Pr})_2$EtN (61% yield). The Stille cross-coupling of **BDY-1** with the corresponding bisstannylthiophene reagents, 2,5-bis(trimethylstannyl)thiophene (**3**) and 5,5′-bis(trimethylstannyl)-2-2′-thiophene (**4**), in toluene using Pd$(PPh_3)_2Cl_2$ as the catalyst yielded semiconductors **BDY-3T-BDY** and **BDY-4T-BDY**, respectively, in 45−50% yields. The new compounds are found to be chemically stable over one year in the solid state, when stored under ambient conditions without excluding light. In addition, they exhibit good solubility (up to 100 mg/mL) in common organic solvents (dichloromethane, chloroform, toluene, and tetrahydrofuran), which enables convenient purification via column chromatography and device fabrication via solution processing. Attempts to purify **BDY-3T-BDY** and **BDY-4T-BDY** via gradient sublimation under high vacuum (2×10^{-5} Torr) failed, resulting in complete decomposition. These data indicate that the new compounds may not be used to fabricate thin films via physical vapor deposition method, which is in line with the poor charge carrier mobilities obtained for the vapor-deposited OTFTs (vide infra). The unusual good solubilities of **BDY-3T-BDY** and **BDY-4T-BDY** despite the absence of long lipophilic alkyl substituents (C_nH_{2n+1}, $n > 4$) may be attributed to inter-ring torsions in solution (vide infra) and large dipole moments of BODIPY moieties, which both facilitate interactions with the solvent molecules. This is in sharp contrast to the design principles of the majority of the *n*-type semiconductors reported to date, which have employed linear/branched lipophilic alkyl substituents to ensure good solubility of strong donor−acceptor π-backbones. Thus, these data demonstrate a unique feature of BODIPY building block in the design of solution-processable molecular semiconductors for facile synthesis/purification.[44] In addition, because alkyl substituents are

DOI: 10.1021/acsami.6b02788
ACS Appl. Mater. Interfaces 2016, 8, 14077−14087

not needed, the density of insulating σ-electrons can be significantly lowered in BODIPY-based semiconductor solid state.

The chemical structures and purity of the new compounds were accessed by ^{1}H NMR, ^{13}C NMR, MALDI-TOF mass spectrometry (MS), and elemental analysis. It is noteworthy that the MALDI-TOF MS analyses of **BDY-3T-BDY** and **BDY-4T-BDY** exhibited up to four different peak groups corresponding to the protonated molecular ions ($[M + H]^+$) and ions formed by rupture of fluorine atom(s) and/or methyl groups ($[M - F]^+$, $[M - 4\times CH_3 - F]^+$, $[M - 4\times CH_3 - 2F]^+$) (Figures S3 and S4).[45] On the basis of conventional melting temperature measurements and differential scanning calorimetry (DSC) analysis, no thermal transitions were observed until decomposition. However, thermogravimetric (TGA) analysis indicates reasonable thermal stability of the new molecules with decomposition thresholds located at ~325 °C (Figure S5).

Optoelectronic Characterizations. The optical and electrochemical characteristics of the new compounds were studied by optical absorption and fluorescence spectroscopies as well as cyclic voltammetry. The corresponding spectra and voltammograms are shown in Figures 3 and S6, and the data are summarized in Table 1. Both compounds exhibit two distinct absorption peaks in THF solution with λ_{max} at 361/526 nm for **BDY-3T-BDY** and at 377/526 nm for **BDY-4T-BDY**. The highly intense absorption peaks observed at 526 nm ($\varepsilon = 2 \times 10^5$ M^{-1} cm^{-1}) along with the out-of-plane vibronic features at 497 nm (at ~1100 cm^{-1} from the absorption maximum) are characteristics of the $\pi-\pi^*$ ($S_0 \rightarrow S_1$) transition of the BODIPY moiety.[46] In addition, this absorption peak matches well with the absorption profile of **BDY-1** (Figure 3A, λ_{max} = 525 nm), and it is nearly identical to that of the model compound **BDY-C11**, with *meso*-alkyl substituents (Figure S6, λ_{max} = 506 nm). Furthermore, no additional lower energy shoulder corresponding to an intramolecular charge transfer process was observed. The broad, higher energy absorption peaks at 361−377 nm are attributed to interplay of lower-intensity BODIPY-based $S_0 \rightarrow S_2$ and oligothiophene-based $\pi-\pi^*$ transitions.

The red-shifted ($\Delta\lambda$ = 16 nm) absorption maximum of **BDY-4T-BDY** for the high-energy region, as compared to that in **BDY-3T-BDY**, correlates well with its further π-extended donor core (quaterthiophene vs terthiophene).[47] These observations indicate minimal ground-state interaction or excitonic coupling between the BODIPY-based π-acceptor and the 3T/4T-based π-donor chromophores in dilute solutions of the present compounds. Therefore, it is very likely that the inter-ring torsional angles between the BODIPY and the *meso*-thiophene units increase in solution ($\theta \gg 48°$) as compared to those in the solid state, giving rise to concomitant decrease of electronic interaction between BODIPY and oligothiophene (3T or 4T) π-orbitals, which leads to distinct absorption profiles of two chromophore units. It is noteworthy that this nonplanar geometry undoubtedly contributes to the superior solubility of the present compounds in common organic solvents.

The poor electronic interaction in the ground state was found to be significantly enhanced in the excited state to facilitate nonradiative decay pathways. Thus, the fluorescence spectra of **BDY-3T-BDY** and **BDY-4T-BDY** in THF solutions (Figure S7) exhibit broad emission peaks with maxima at 652 and 678 nm, respectively, corresponding to large Stokes shifts of 126−152 nm. The fluorescence quantum yields (Φ_F) were measured as 0.037 (**BDY-3T-BDY**) and 0.053 (**BDY-4T-**

Table 1. Summary of Thermal, Optical Absorption, Emission, and Electrochemical Properties of Compounds BDY-3T-BDY and BDY-4T-BDY and Corresponding Estimated Frontier Molecular Orbital Energies

compound	T_{TGA}[a] (°C)	$\lambda_{abs}^{sol.}$ (nm) (E_g (eV))[b]	λ_{abs}^{film} (nm) (E_g (eV))[c]	$\lambda_{em}^{sol.}$ (nm)[d]	$E_{red\text{-}1,2}^{1/2}$ (V)[e]	E_{LUMO} (eV)[f]	E_{HOMO} (eV)[g]
BDY-3T-BDY	325	361, 526 (2.23 eV)	349, 555 (1.94 eV)	652 (Φ_F = 0.037) in THF, 630 (Φ_F = 0.043) in toluene	−0.74, −0.84	−3.66	−5.89
BDY-4T-BDY	325	377, 526 (2.19 eV)	376, 565 (1.94 eV)	678 (Φ_F = 0.053) in THF, 630 (Φ_F = 0.055) in toluene	−0.73, −0.85	−3.67	−5.86

[a]Onset decomposition temperature measured by TGA under nitrogen at a scan rate of 10 °C/min. [b]From optical absorption in THF, optical band gap is estimated from the low energy band edge of the UV−vis absorption spectrum. [c]From optical absorption as spin-coated thin film on glass, optical band gap is estimated from the low-energy band edge of the UV−vis absorption spectrum. [d]From fluorescence spectra in THF or toluene; the fluorescence quantum yield values were determined by comparing with the fluorescence of Rhodamine 6G as the standard (Φ_F = 0.76 in water). [e]Measured in 0.1 M $Bu_4N^+PF_6^-$ in THF at a scan rate of 50 mV/s (vs Ag/AgCl). [f]Estimated from the equation $E_{LUMO} = -4.40$ eV $- E_{red}^{1/2}$. [g]E_{HOMO} is calculated from $E_g = E_{LUMO} - E_{HOMO}$.

DOI: 10.1021/acsami.6b02788
ACS Appl. Mater. Interfaces 2016, 8, 14077−14087

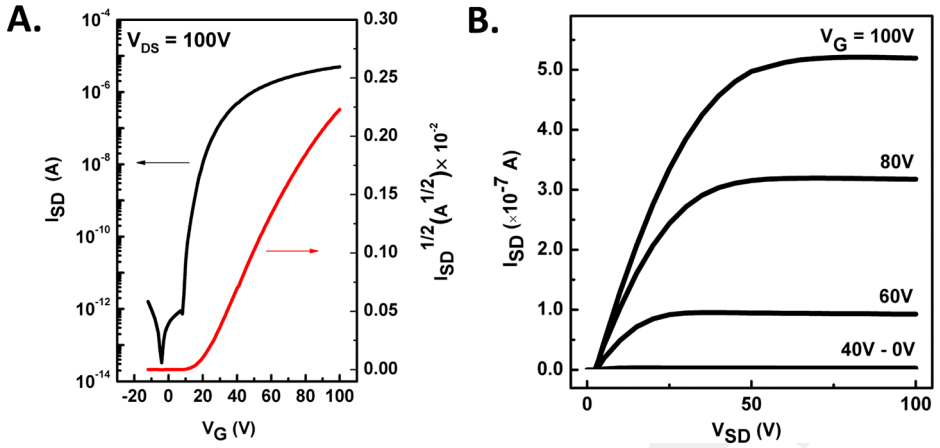

Figure 4. Representative OTFT transfer (A) and output (B) plots for devices fabricated with solution-sheared **BDY-4T-BDY** thin films.

Table 2. Organic Thin-Film Transistor Characteristics Based on Thin Films of BDY-3T-BDY and BDY-4T-BDY[a,b]

compound	method	μ ($cm^2/(V\ s)$)	V_T (V)	I_{on}/I_{off}	SS (V/dec)	N_T (cm^{-2})
BDY-3T-BDY	vacuum deposition	1.7×10^{-4}	37	9.0×10^7	32.2	1.2×10^{12}
	solution shear	2.7×10^{-4}	43	9.6×10^5	17.9	2.1×10^{12}
BDY-4T-BDY	vacuum deposition	5.3×10^{-4}	75	3.5×10^5	18.4	1.7×10^{12}
	solution shear	0.011	19	1.5×10^8	9.35	7.4×10^{11}

[a]The OTFT electrical characteristics were measured in a vacuum probe station ($P < 10^{-5}$ Torr). [b]The mobility values, threshold voltages, and I_{on}/I_{off} ratios given are the average values for 10 devices with the standard deviations of less than 5%.

BDY). The observed broad emission peaks, large Stokes shifts, and relatively low quantum yields are in contrast to typical BODIPY emission characteristics, and they are indicative of the presence of intramolecular energy-/charge-transfer based nonradiative pathways in the excited state.[44] Although the absorption spectra of the current compounds are nearly invariant across several solvents, their corresponding fluorescence spectra exhibit positive solvachromatisms (λ_{em} = 630 nm → 652−678 nm; Φ_F = 0.043−0.055 → 0.037−0.053 for toluene (ε = 2.3) → THF (ε = 7.6)) with increasing solvent polarity, associated with concomitant peak broadening and a decreased quantum yield. These observations further support that the final relaxed excited states may have larger dipole moments as a result of charge transfer (CT) between subchromophoric units (Figure S7). Similar charge-transfer behaviors were observed in the emissive characteristics of previously reported BODIPY dyads.[48]

UV−vis absorption spectra of the corresponding thin films do not show the obvious BODIPY profiles and exhibit broad and red-shifted maxima at 555 and 565 nm for **BDY-3T-BDY** and **BDY-4T-BDY**, respectively. In the solid state, the low-energy absorption edges exhibit significant bathochromic shifts ($\Delta\lambda$ = 75−80 nm) with onsets located at 635−640 nm indicating reduced solid-state optical band gaps (~1.94 eV) versus those measured in solution. This result points to enhanced π-core planarization and intermolecular interactions, and some degree of electronic coupling between donor and acceptor subunits in the solid state. The red-shift in **BDY-4T-BDY** ($\Delta\lambda$ = 39 nm) is more pronounced than that in **BDY-3T-BDY** ($\Delta\lambda$ = 29 nm), probably reflecting the difference in solid-state ordering levels between these semiconductors and enhanced donor strength of quaterthiophene versus terthiophene.

On the basis of the cyclic voltammetry (CV) measurements in THF solution, both molecules undergo two reversible reductions with the first and second half-wave potentials ($E_{red}^{1/2}$) located at −0.74/−0.84 V (vs Ag/AgCl) for **BDY-3T-BDY** and −0.73/−0.85 V (vs Ag/AgCl) for **BDY-4T-BDY** (Figure 3B). The reversibility of the two reduction processes indicates the good redox stability of the new BODIPY-based molecules. From the CV data, the HOMO/LUMO energy levels are estimated as −3.66/−5.89 eV and −3.67/−5.86 eV for **BDY-3T-BDY** and **BDY-4T-BDY**, respectively. The experimental LUMO energies are in the range of those observed for previously reported *n*-channel semiconductors (−2.9 eV to −4.3 eV), which is in line with the theoretical results. Considering the observed stable *n*-doping/undoping profiles and LUMO energetics, the new molecules are potential *n*-channel semiconductors.

Thin-Film Transistor Characterization. The semiconductor characteristics of **BDY-3T-BDY** and **BDY-4T-BDY** were measured in a top-contact/bottom-gate (TC-BG) organic thin-film transistor (OTFT) device architecture. The semiconductor thin-films (40−60 nm for vapor deposited film, 300−600 nm for solution processed film) were deposited via physical vapor deposition and solution-shearing methods on pretreated n^{+2}-Si/SiO_2 (300 nm) gate-dielectric substrates. The dielectric surface was functionalized either with a self-assembled monolayer (SAM) for vapor-deposition or with polymer brushes for solution-shearing to achieve a favorable semiconductor−dielectric interface.[49−53] Typical transfer and output plots are shown in Figures 4 and S8−S10, and the OTFT device characteristics are summarized in Tables 2 and S2.

As a first approach, **BDY-3T-BDY** and **BDY-4T-BDY** semiconductor films were grown by physical vapor deposition under high vacuum (~2×10^{-5} Torr) at different substrate temperatures (T_D) of 25, 50, and 80 °C. Although vapor-deposited thin-films of both semiconductors fabricated on n^{+2}-Si/SiO_2 substrates that maintained a temperature, T_D, of 80 °C were inactive, the devices fabricated at room temperature (T_D =

DOI: 10.1021/acsami.6b02788
ACS Appl. Mater. Interfaces 2016, 8, 14077−14087

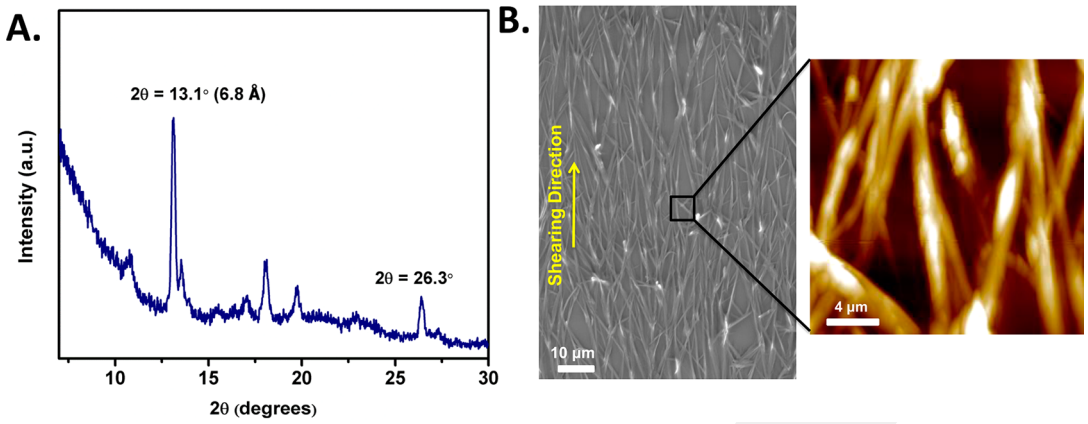

Figure 5. (A) θ–2θ X-ray diffraction (XRD) scans of solution-sheared **BDY-4T-BDY** films. (B) Top-view SEM (left) and AFM topographic images (right) of solution-sheared **BDY-4T-BDY** films indicating the solution-shearing and major fiber alignment directions.

25 °C) showed a weak *n*-channel behavior with electron mobilities of 2×10^{-4} to 5×10^{-4} $cm^2/V{\cdot}s$ (Figures S8 and S9, and Table S2), irrespective of surface treatment for the gate dielectric. Next, solution processing of the semiconductor was employed to fabricate the OTFT devices, and among various approaches, solution-shearing was preferred to achieve unidirectional crystalline semiconductor microstructure with favorable carrier transport characteristics.[54] The solution-shearing process was optimized with regards to the solvent type, substrate temperature, and shearing speed to fine-tune the rate of semiconductor crystallization in thin-film phase.[55] The optimal conditions were identified as using chlorobenzene solutions (1 mg/mL) at a substrate temperature of 50–60 °C and shearing speed of 0.3–1 mm/min for both semiconductors. Solution-sheared films of both compounds exhibited typical *n*-channel transport characteristics with those of **BDY-3T-BDY** displaying an electron mobility of 2.7×10^{-4} $cm^2/(V\ s)$, which is similar to those obtained for vapor-deposited films (Figure S10). However, **BDY-4T-BDY**-based solution-sheared thin-films, which include a relatively longer quaterthiophene π-donor part, exhibited higher device performance than those of **BDY-3T-BDY** with shorter π-donor of terthiophene. The OTFTs fabricated with **BDY-4T-BDY** showed electron mobility as high as 0.011 $cm^2/V{\cdot}s$ with an impressive current on/off ratio of $>10^8$ (Figure 4). Note that this electron mobility is obtained for devices having the source-drain electrodes deposited perpendicular to the major fiber alignment direction (vide infra). To the best of our knowledge, this is the highest OTFT device performance reported to date for a BODIPY-based small molecule.[56] The extremely low off current ($\sim 10^{-13}$ A) and the high $I_{on/off}$ ratio ($>10^8$) point to the favorable current modulation characteristics of **BDY-4T-BDY** thin-films. The higher electron mobility of solution-sheared **BDY-4T-BDY** thin-films correlates well with its relatively lower charge-carrier trap density ($N_T = 7.4 \times 10^{11}$ cm^{-2}) among the current BODIPY-based OTFT devices, which leads to more favorable charge-transport (Tables 2 and S2).[57−59]

Thin-Film Microstructure and Morphology. The microstructure and morphology of the present semiconductor thin-films were studied by θ–2θ X-ray diffraction (XRD), atomic force microscopy (AFM), and scanning electron microscopy (SEM) to rationalize the observed device performances. The corresponding XRD profiles and AFM/SEM images are shown in Figures 5 and S11–S16. XRD scans reveal that vapor-deposited thin-films of both semiconductors and solution-sheared thin-films of **BDY-3T-BDY** are essentially amorphous (Figures S11–S13), and that only the solution-sheared thin-film of **BDY-4T-BDY** is highly textured (Figure 5). For solution-sheared thin-films of **BDY-4T-BDY**, no first-order reflection was observed at low-angles ($2\theta < 10°$), which indicates the absence of typical edge-on molecular long-axis orientation on the substrate. On the basis of the computed molecular lengths (~2.4 nm), one would expect to see the first-order diffraction peak at $2\theta \approx 4–5°$ if the molecules are oriented with their long axis along the substrate normal. However, a major reflection is observed at $2\theta = 13.1°$ along with the second-order peak at $2\theta = 26.4°$, which shows that **BDY-4T-BDY** thin-films include a major crystalline phase with an interlayer *d*-spacing of 6.8 Å along the substrate normal. This is much smaller than the computed long-axis molecular lengths (~2.4 nm), and consistent with the computed length of **BDY-4T-BDY** along the short molecular axis (~7 Å). Therefore, it is very likely that BODIPY-based molecules adopt an unusual molecular packing in the thin-film phase, either featuring a highly tilted molecular orientation on the substrate ($\theta > 70°$) or, more likely, aligning with their short axis along the substrate normal. Note that self-assembly of **BDY-4T-BDY** semiconductor molecules into well-defined microfibers (vide infra) in thin-film phase is more consistent with the short-axis molecular orientation, which enables strong π–π interactions along the fiber long-axis.[60] A secondary crystalline phase ($2\theta = 13.6°$) with a lower intensity and additional higher angle diffraction peaks at $2\theta = 18.1°$ and 19.8° were also evident from the XRD spectra. Although end-functionalized oligothiophenes such α,ω-dihexyl-terthiophene and α,ω-dihexyl-quaterthiophene typically show long-axis molecular edge-on orientations on various dielectrics including polymeric surfaces,[61,62] the current rather unusual thin-film microstructure is probably due to the chemical nature of BODIPY end-units and the absence of long lipophilic alkyl substituents, which both influence the current semiconductor physisorption characteristics on the polymeric dielectric surface.

The AFM and top-view SEM images were recorded to characterize the film surface morphology.[63] As shown in Figure 5B, the surface topology of solution-sheared **BDY-4T-BDY** thin film shows anisotropic micrometer-sized crystalline fiber structures that grow along the shearing direction. The widths of the microfibers were as large as 1–2 μm, and their lengths can reach to ~0.1 mm. As seen from the optical microscopy images (Figure S14), these microfibers exhibit a directional and

DOI: 10.1021/acsami.6b02788
ACS Appl. Mater. Interfaces 2016, 8, 14077−14087

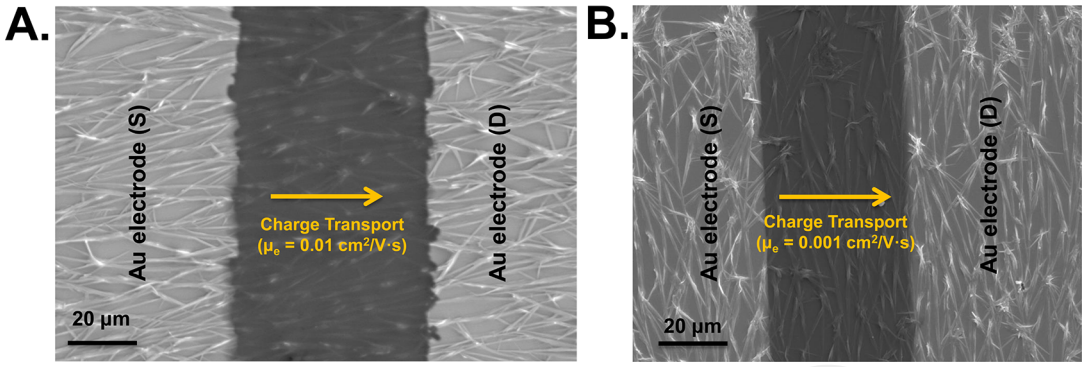

Figure 6. Top-view SEM images of OTFT devices fabricated via solution shearing of **BDY-4T-BDY** with source-drain electrodes deposited perpendicular (A) and parallel (B) to the major fiber alignment direction.

highly homogeneous distribution in an area of 1 mm × 1 mm, and they are aligned mainly along the shearing direction. Close inspection of these fibers via AFM indicates the presence of grain bundles with much smaller dimensions (∼100−200 nm), giving information about the mechanism of how these fibers form. Because uniaxially aligned fiber-based semiconductor morphologies were obtained with **BDY-4T-BDY**-based films, charge carrier mobilities were measured in two different source-drain electrode configurations with electrodes being deposited perpendicular or parallel to the major fiber alignment direction. As shown in Figure 6B, electron mobilities of 0.001 cm^2/V·s (Figure S15) were measured for the OTFTs with the charge-transport direction perpendicular to the major fiber alignment direction. This mobility value is 1 order of magnitude lower than the electron mobilities measured in OTFTs having charge-transport along the major fiber alignment direction (Figure 6A), indicating the presence of fiber-alignment-induced charge-transport anisotropy ($\mu_{\parallel}/\mu_{\perp} \approx 10$). Similar anisotropic charge-transport properties were observed with highly oriented semiconducting polymers;[64,65] thus the alignment of semiconducting fibers along the conduction channel is very crucial to enhance macroscopic charge-transport.[66]

The solution-processed thin-films of **BDY-3T-BDY** showed fiber-like, randomly aligned anisotropic features with much smaller widths and lengths as compared to those of **BDY-4T-BDY** (Figure S16). The interconnectivity between these features was found to be poor as compared to that of **BDY-4T-BDY**. On the other hand, vacuum-deposited thin-films of **BDY-3T-BDY** and **BDY-4T-BDY** showed completely different morphologies with relatively smooth (RMS surface roughness <9.1 nm for 5.0 μm × 5.0 μm scan area) and isotropic spherulites of ∼100 nm in diameter (Figures S17 and S18). Therefore, on the contrary of **BDY-4T-BDY** solution-sheared films, the absence of thin-film texturing and poor film morphology are consistent with the poor electron mobility of these semiconductor films.

4. CONCLUSION

We have demonstrated the design, synthesis, and characterization of a new class of BODIPY-based semiconductors (**BDY-3T-BDY** and **BDY-4T-BDY**) with an acceptor−donor−acceptor (A−D−A) molecular architecture. The structural, optoelectronic, and physicochemical properties of the new semiconductors were investigated in details. Single-crystal XRD characterization of the key intermediate, **BDY-1**, reveals crucial structural properties. Top-contact/bottom-gate OTFTs were fabricated with these semiconductors, and relatively high electron mobilities of 0.01 cm^2/V·s and excellent current on/off ratios of >10^8 have been obtained for solution-processed semiconductor films. To the best of our knowledge, these values are the highest reported to date for a BODIPY-based small molecular OTFT semiconductor. The microstructural and morphological characterizations of the new semiconductor thin-films explain the observed relatively high charge carrier mobilities. Specifically, for **BDY-4T-BDY**-based thin-films, highly crystalline, relatively long (∼0.1 mm), and micrometer-sized (1−2 μm) fibers were obtained along the shearing direction from source to drain, which allows for efficient long-range S → D charge-transport. This result is consistent with its relatively high electron mobility among the present semiconductor films. In addition, fiber-alignment-induced charge-transport anisotropy ($\mu_{\parallel}/\mu_{\perp} \approx 10$) was observed resulting in 1 order of magnitude difference in electron mobilities of solution-sheared semiconductor films. Undoubtedly, our results provide important guidelines for designing BODIPY-based molecular semiconductors, indicating that through rational design and synthesis, BODIPY can be a highly favorable building block for efficient electron charge-transport in solution-processed opto-electronics.

■ ASSOCIATED CONTENT

Ⓢ Supporting Information

The Supporting Information is available free of charge on the ACS Publications website at DOI: 10.1021/acsami.6b02788.

Synthetic procedures and characterizations for compounds **2**−**4**, Scheme 1, Figures S1−S18, and Tables S1 and S2 (PDF)

■ AUTHOR INFORMATION

Corresponding Authors

*E-mail: afacchetti@polyera.com.
*E-mail: choongik@sogang.ac.kr.
*E-mail: hakan.usta@agu.edu.tr.

Author Contributions

#M.O. and D.C. contributed equally to this work.

Notes

The authors declare no competing financial interest.

■ ACKNOWLEDGMENTS

This work was supported by the Scientific and Technological Research Council of Turkey (TUBITAK) grant number 114M226. H.U. acknowledges support from The Science Academy, Young Scientist Award Program (BAGEP 2014),

DOI: 10.1021/acsami.6b02788
ACS Appl. Mater. Interfaces 2016, 8, 14077−14087

and Turkish Academy of Sciences, The Young Scientists Award Program (TUBA-GEBİP 2015). C.K. acknowledges support from the Basic Science Research Program through the National Research Foundation of Korea (NRF) (NRF-2014R1A1A1A05002158). This project was funded by the Deanship of Scientific Research (DSR), King Abdulaziz University, Jeddah, under grant no. (80-130-35-HiCi).

REFERENCES

(1) Benniston, A. C.; Copley, G.; Harriman, A.; Rewinska, D. B.; Harrington, R. W.; Clegg, W. A. Donor−Acceptor Molecular Dyad Showing Multiple Electronic Energy-Transfer Processes in Crystalline and Amorphous States. *J. Am. Chem. Soc.* **2008**, *130*, 7174−7175.

(2) Bonaccorsi, P.; Aversa, M. C.; Barattucci, A.; Papalia, T.; Puntoriero, F.; Campagna, S. Artificial Light-Harvesting Antenna Systems Grafted on a Carbohydrate Platform. *Chem. Commun.* **2012**, *48*, 10550−10552.

(3) El-Khouly, M. E.; Wijesinghe, C. A.; Nesterov, V. N.; Zandler, M. E.; Fukuzumi, S.; D'Souza, F. Ultrafast Photoinduced Energy and Electron Transfer in Multi-Modular Donor-Acceptor Conjugates. *Chem. - Eur. J.* **2012**, *18*, 13844−13853.

(4) Niu, L.; Guan, Y.; Chen, Y.; Wu, L.; Tung, C.; Yang, Q. BODIPY-Based Ratiometric Fluorescent Sensor for Highly Selective Detection of Glutathione over Cysteine and Homocysteine. *J. Am. Chem. Soc.* **2012**, *134*, 18928−18931.

(5) Loudet, A.; Burgess, K. BODIPY Dyes and Their Derivatives: Syntheses and Spectroscopic Properties. *Chem. Rev.* **2007**, *107*, 4891−4932.

(6) Gomez-Duran, C. F. A.; Hu, R.; Feng, G.; Li, T.; Bu, F.; Arseneault, M.; Liu, B.; Peña-Cabrera, E.; Tang, B. Z. Effect of AIE Substituents on the Fluorescence of Tetraphenylethene-Containing BODIPY Derivatives. *ACS Appl. Mater. Interfaces* **2015**, *7*, 15168−15176.

(7) Bessette, A.; Hanan, G. S. Design, Synthesis and Photophysical Studies of Dipyrromethene-Based Materials: Insights into Their Applications in Organic Photovoltaic Devices. *Chem. Soc. Rev.* **2014**, *43*, 3342−3405.

(8) Boens, N.; Leen, V.; Dehaen, W. Fluorescent Indicators Based on BODIPY. *Chem. Soc. Rev.* **2012**, *41*, 1130−1172.

(9) Liu, W.; Tang, A.; Chen, J.; Wu, Y.; Zhan, C.; Yao, J. Photocurrent Enhancement of BODIPY-Based Solution-Processed Small-Molecule Solar Cells by Dimerization via the Meso Position. *ACS Appl. Mater. Interfaces* **2014**, *6*, 22496−22505.

(10) Chen, J. J.; Conron, S. M.; Erwin, P.; Dimitriou, M.; McAlahney, K.; Thompson, M. E. High-Efficiency BODIPY-Based Organic Photovoltaics. *ACS Appl. Mater. Interfaces* **2015**, *7*, 662−669.

(11) Cortizo-Lacalle, D.; Howells, C. T.; Pandey, U. K.; Cameron, J.; Findlay, N. J.; Inigo, A. R.; Tuttle, T.; Skabara, P. J.; Samuel, I. D. W. Solution Processable Diketopyrrolopyrrole (DPP) Cored Small Molecules with BODIPY End Groups as Novel Donors for Organic Solar Cells. *Beilstein J. Org. Chem.* **2014**, *10*, 2683−2695.

(12) Zhu, W.; Zheng, R.; Fu, X.; Fu, H.; Shi, Q.; Zhen, Y.; Dong, H.; Hu, W. Revealing the Charge-Transfer Interactions in Self-Assembled Organic Cocrystals: Two-Dimensional Photonic Applications. *Angew. Chem., Int. Ed.* **2015**, *54*, 6785−6789.

(13) Ji, D.; Jiang, L.; Dong, H.; Meng, Q.; Zhen, Y.; Hu, W. Silver Mirror Reaction for Organic Electronics: Towards High-Performance Organic Field-Effect Transistors and Circuits. *J. Mater. Chem. C* **2014**, *2*, 4142−4146.

(14) Bura, T.; Leclerc, N.; Fall, S.; Lévêque, P.; Heiser, T.; Retailleau, P.; Rihn, S.; Mirloup, A.; Ziessel, R. High-Performance Solution-Processed Solar Cells and Ambipolar Behavior in Organic Field-Effect Transistors with Thienyl-BODIPY Scaffoldings. *J. Am. Chem. Soc.* **2012**, *134*, 17404−17407.

(15) Poe, A. M.; Pelle, A. M. D.; Subrahmanyam, A. V.; White, W.; Wantz, G.; Thayumanavan, S. Small Molecule BODIPY Dyes as Non-Fullerene Acceptors in Bulk Heterojunction Organic Photovoltaics. *Chem. Commun.* **2014**, *50*, 2913−2915.

(16) Usta, H.; Yilmaz, M. D.; Avestro, A.-J.; Boudinet, D.; Denti, M.; Zhao, W.; Stoddart, J. F.; Facchetti, A. BODIPY−Thiophene Copolymers as *p*-Channel Semiconductors for Organic Thin-Film Transistors. *Adv. Mater.* **2013**, *25*, 4327−4334.

(17) Ozdemir, M.; Choi, D.; Kwon, G.; Zorlu, Y.; Kim, H.; Kim, M.-G.; Seo, S. Y.; Sen, U.; Citir, M.; Kim, C.; Usta, H. Design, Synthesis, and Characterization of α,ω-Disubstituted Indeno[1,2-b]fluorene-6,12-dione-Thiophene Molecular Semiconductors. Enhancement of Ambipolar Charge Transport Through Synthetic Tailoring of Alkyl Substituents. *RSC Adv.* **2016**, *6*, 212−226.

(18) Facchetti, A. π-Conjugated Polymers for Organic Electronics and Photovoltaic Cell Applications. *Chem. Mater.* **2011**, *23*, 733−758.

(19) Ebata, H.; Izawa, T.; Miyazaki, E.; Takimiya, K.; Ikeda, M.; Kuwabara, H.; Yui, T. Highly Soluble [1]Benzothieno[3,2-b]-benzothiophene (BTBT) Derivatives for High-Performance, Solution-Processed Organic Field-Effect Transistors. *J. Am. Chem. Soc.* **2007**, *129*, 15732−15733.

(20) Izawa, T.; Miyazaki, E.; Takimiya, K. Molecular Ordering of High-Performance Soluble Molecular Semiconductors and Re-evaluation of Their Field-Effect Transistor Characteristics. *Adv. Mater.* **2008**, *20*, 3388−3392.

(21) Reyes-Martinez, M. A.; Crosby, A. J.; Briseno, A. L. Rubrene Crystal Field-Effect Mobility Modulation via Conductive Channel Wrinkling. *Nat. Commun.* **2015**, *6*, 6948.

(22) Zhang, Y.; Wise, A. J.; Barnes, M. D.; Briseno, A. L. A Forrest of Crystals. *Mater. Today* **2014**, *17*, 464−465.

(23) Vercelli, B.; Pasini, M.; Berlin, A.; Casado, J.; Navarrete, J. T. L.; Ortiz, R. P.; Zotti, G. Phenyl- and Thienyl-Ended Symmetric Azomethines and Azines as Model Compounds for n-Channel Organic Field-Effect Transistors: An Electrochemical and Computational Study. *J. Phys. Chem. C* **2014**, *118*, 3984−3993.

(24) Ortiz, R. P.; Herrera, H.; Blanco, R.; Huang, H.; Facchetti, A.; Marks, T. J.; Zheng, Y.; Segura, J. L. Organic n-Channel Field-Effect Transistors Based on Arylenediimide-Thiophene Derivatives. *J. Am. Chem. Soc.* **2010**, *132*, 8440−8452.

(25) Li, G.; Kang, C.; Gong, X.; Zhang, J.; Li, W.; Li, C.; Dong, H.; Hu, W.; Bo, Z. 5,6-Difluorobenzothiadiazole and Silafluorene Based Conjugated Polymers for Organic Photovoltaic Cells. *J. Mater. Chem. C* **2014**, *2*, 5116−5123.

(26) Turrisi, R.; Sanguineti, A.; Sassi, M.; Savoie, B.; Takai, A.; Patriarca, G. E.; Salamone, M. M.; Ruffo, R.; Vaccaro, G.; Meinardi, F.; Marks, T. J.; Facchetti, A.; Beverina, L. Stokes shift/emission Efficiency Trade-off in Donor−Acceptor Perylenemonoimides for Luminescent Solar Concentrators. *J. Mater. Chem. A* **2015**, *3*, 8045−8054.

(27) Meinardi, F.; Colombo, A.; Velizhanin, K. A.; Simonutti, R.; Lorenzon, M.; Beverina, L.; Viswanatha, R.; Klimov, V. I.; Brovelli, S. Large-Area Luminescent Solar Concentrators Based on 'Stokes-Shift-Engineered' Nanocrystals in a Mass-Polymerized PMMA Matrix. *Nat. Photonics* **2014**, *8*, 392−399.

(28) Sanguineti, A.; Sassi, M.; Turrisi, R.; Ruffo, R.; Vaccaro, G.; Meinardi, F.; Beverina, L. High Stokes Shift Perylene Dyes for Luminescent Solar Concentrators. *Chem. Commun.* **2013**, *49*, 1618−1620.

(29) Ortiz, R. P.; Yan, H.; Facchetti, A.; Marks, T. J. Azine- and Azole-Functionalized Oligó and Polythiophene Semiconductors for Organic Thin-Film Transistors. *Materials* **2010**, *3*, 1553−1558.

(30) Beverina, L.; Pagani, G. A. π-Conjugated Zwitterions as Paradigm of Donor−Acceptor Building Blocks in Organic-Based Materials. *Acc. Chem. Res.* **2014**, *47*, 319−329.

(31) Frisch, M. J.; Trucks, G. W.; Schlegel, H. B.; Scuseria, G. E.; Robb, M. A.; Cheeseman, J. R.; Scalmani, G.; Barone, V.; Mennucci, B.; Petersson, G. A.; Nakatsuji, H.; Caricato, M.; Li, X.; Hratchian, H. P.; Izmaylov, A. F.; Bloino, J.; Zheng, G.; Sonnenberg, J. L.; Hada, M.; Ehara, M.; Toyota, K.; Fukuda, R.; Hasegawa, J.; Ishida, M.; Nakajima, T.; Honda, Y.; Kitao, O.; Nakai, H.; Vreven, T.; Montgomery, J. A., Jr.; Peralta, J. E.; Ogliaro, F.; Bearpark, M.; Heyd, J. J.; Brothers, E.; Kudin, K. N.; Staroverov, V. N.; Keith, T.; Kobayashi, R.; Normand, J.; Raghavachari, K.; Rendell, A.; Burant, J. C.; Iyengar, S. S.; Tomasi, J.; Cossi, M.; Rega, N.; Millam, J. M.; Klene, M.; Knox, J. E.; Cross, J. B.;

DOI: 10.1021/acsami.6b02788
ACS Appl. Mater. Interfaces 2016, 8, 14077−14087

Bakken, V.; Adamo, C.; Jaramillo, J.; Gomperts, R.; Stratmann, R. E.; Yazyev, O.; Austin, A. J.; Cammi, R.; Pomelli, C.; Ochterski, J. W.; Martin, R. L.; Morokuma, K.; Zakrzewski, V. G.; Voth, G. A.; Salvador, P.; Dannenberg, J. J.; Dapprich, S.; Daniels, A. D.; Farkas, O.; Foresman, J. B.; Ortiz, J. V.; Cioslowski, J.; Fox, D. J. *Gaussian 09*, revision C.01; Gaussian, Inc.: Wallingford, CT, 2010.
(32) Bruker. *APEX2, version 2014.11-0*; Bruker AXS Inc.: Madison, WI, 2014.
(33) Bruker. *SAINT, version V8.34A*; Bruker AXS Inc.: Madison, WI, 2013.
(34) Bruker. *SADABS, version 2014/5*; Bruker AXS Inc.: Madison, WI, 2014.
(35) Bruker. *SHELXTL, version 6.14*; Bruker AXS Inc.: Madison, WI, 2010.
(36) Spek, A. L. Structure Validation in Chemical Crystallography. *Acta Crystallogr., Sect. D: Biol. Crystallogr.* **2009**, *D65*, 148−155.
(37) Macrae, C. F.; Edgington, P. R.; McCabe, P.; Pidcock, E.; Shields, G. P.; Taylor, R.; Towler, M.; Van de Streek, J. Mercury: Visualization and Analysis of Crystal Structures. *J. Appl. Crystallogr.* **2006**, *39*, 453−457.
(38) Yang, Y.; Guo, Q.; Chen, H.; Zhou, Z.; Guo, Z.; Shen, Z. Thienopyrrole-Expanded BODIPY as a Potential NIR Photosensitizer for Photodynamic Therapy. *Chem. Commun.* **2013**, *49*, 3940−3942.
(39) Fabiano, S.; Usta, H.; Forchheimer, R.; Crispin, X.; Facchetti, A.; Berggren, M. Selective Remanent Ambipolar Charge Transport in Polymeric Field-Effect Transistors For High- Performance Logic Circuits Fabricated in Ambient. *Adv. Mater.* **2014**, *26*, 7438−7443.
(40) Choi, J.; Kim, K.-H.; Yu, H.; Lee, C.; Kang, H.; Song, I.; Kim, Y.; Oh, J. H.; Kim, B. J. Importance of Electron Transport Ability in Naphthalene Diimide-Based Polymer Acceptors for High-Performance, Additive-Free, All-Polymer Solar Cells. *Chem. Mater.* **2015**, *27*, 5230−5237.
(41) Usta, H.; Newman, C.; Chen, Z.; Facchetti, A. Dithienocoronenediimide-Based Copolymers as Novel Ambipolar Semiconductors for Organic Thin Film Transistors. *Adv. Mater.* **2012**, *24*, 3678−3684.
(42) Chen, Z.; Zheng, Y.; Yan, H.; Facchetti, A. Naphthalenedicarboximide- vs Perylenedicarboximide-Based Copolymers. Synthesis and Semiconducting Properties in Bottom-Gate N-Channel Organic Transistors. *J. Am. Chem. Soc.* **2009**, *131*, 8−9.
(43) Usta, H.; Sheets, C.; Denti, M.; Generali, G.; Capelli, R.; Lu, S.; Yu, X.; Muccini, M.; Facchetti, A. Perfluoroalkyl-Functionalized Thiazole-Thiophene Oligomers as N-Channel Semiconductors in Organic Field-Effect and Light-Emitting Transistors. *Chem. Mater.* **2014**, *26*, 6542−6556.
(44) Liu, X.; Wang, Y.; Gao, J.; Jiang, L.; Qi, X.; Hao, W.; Zou, S.; Zhang, H.; Li, H.; Hu, W. Easily Solution-Processed, High-Performance Microribbon Transistors Based on a 2D Condensed Benzothiophene Derivative. *Chem. Commun.* **2014**, *50*, 442−444.
(45) Sengul, I. F.; Okutan, E.; Kandemir, H.; Astarci, E.; Cosut, B. Carbazole Substituted BODIPY Dyes: Synthesis, Photophysical Properties and Antitumor Activity. *Dyes Pigm.* **2015**, *123*, 32−38.
(46) Benniston, A. C.; Copley, G.; Harriman, A.; Ryan, R. Thermoresponsive Fluorescent Polymers Based on a Quaterthiophene-Containing Boron Dipyrromethene (Bodipy) Dyad Dispersed in Silicone Rubber. *J. Mater. Chem.* **2011**, *21*, 2601−2608.
(47) Zrig, S.; Rémy, P.; Andrioletti, B.; Rose, E.; Asselberghs, I.; Clays, K. Engineering Tuneable Light-Harvesting Systems with Oligothiophene Donors and Mono- or Bis-Bodipy Acceptors. *J. Org. Chem.* **2008**, *73*, 1563−1566.
(48) Whited, M. T.; Patel, N. M.; Roberts, S. T.; Allen, K.; Djurovich, P. I.; Bradforth, S. E.; Thompson, M. E. Symmetry-Breaking Intramolecular Charge Transfer in the Excited State of Meso-Linked BODIPY Dyads. *Chem. Commun.* **2012**, *48*, 284−286.
(49) Kim, C.; Facchetti, A.; Marks, T. J. Gate Dielectric Microstructural Control of Pentacene Film Growth Mode and Field-Effect Transistor Performance. *Adv. Mater.* **2007**, *19*, 2561−2566.
(50) Kobayashi, S.; Nishikawa, T.; Takenobu, T.; Mori, S.; Shimoda, T.; Mitani, T.; Shimotani, H.; Yoshimoto, N.; Ogawa, S.; Iwasa, Y. Control of Carrier Density by Self-Assembled Monolayers in Organic Field-Effect Transistors. *Nat. Mater.* **2004**, *3*, 317−322.
(51) Mühlenen, A. von; Castellani, M.; Schaer, M.; Zuppiroli, L. Controlling Charge-Transfer at the Gate Interface of Organic Field-Effect Transistors. *Phys. Status Solidi B* **2008**, *245*, 1170−1174.
(52) Pernstich, K. P.; Haas, S.; Oberhoff, D.; Goldmann, C.; Gundlach, D. J.; Batlogg, B.; Rashid, A. N.; Schitter, G. Threshold Voltage Shift in Organic Field Effect Transistors by Dipole Monolayers on the Gate Insulator. *J. Appl. Phys.* **2004**, *96*, 6431−6438.
(53) Park, S. H.; Lee, H. S.; Kim, J.-D.; Breiby, D. W.; Kim, E.; Park, Y. D.; Ryu, D. Y.; Lee, D. R.; Cho, J. H. A Polymer Brush Organic Interlayer Improves the Overlying Pentacene Nanostructure and Organic Field-Effect Transistor Performance. *J. Mater. Chem.* **2011**, *21*, 15580−15586.
(54) Giri, G.; Verploegen, E.; Mannsfeld, S. C. B.; Evrenk, S. A.; Kim, D. H.; Lee, S. Y.; Becerril, H. A.; Aspuru-Guzik, A.; Toney, M. F.; Bao, Z. Tuning Charge Transport in Solution-Sheared Organic Semiconductors Using Lattice Strain. *Nature* **2011**, *480*, 504−508.
(55) Liu, Z.; Becerril, H. A.; Roberts, M. E.; Nishi, Y.; Bao, Z. Experimental Study and Statistical Analysis of Solution-Shearing Processed Organic Transistors Based on an Asymmetric Small-Molecule Semiconductor. *IEEE Trans. Electron Devices* **2009**, *56*, 176−185.
(56) Wang, Y.; Chen, J.; Zhen, Y.; Jiang, H.; Yu, G.; Liu, Y.; Baranoff, E.; Tan, H.; Zhu, W. Synthesis and Properties of Novel Near-Infrared Dye Based on BODIPY and Diketopyrrolopyrrole Units. *Mater. Lett.* **2015**, *139*, 130−133.
(57) McDowell, M.; Hill, I. G.; McDermott, J. E.; Bernasek, S. L.; Schwartz, J. Improved Organic Thin-Film Transistor Performance Using Novel Self-Assembled Monolayers. *Appl. Phys. Lett.* **2006**, *88*, 073505.
(58) Klauk, H. Organic Thin-Film Transistors. *Chem. Soc. Rev.* **2010**, *39*, 2643−2666.
(59) Cheng, S.-S.; Huang, P.-Y.; Ramesh, M.; Chang, H.-C.; Chen, L.-M.; Yeh, C.-M.; Fung, C.-L.; Wu, M.-C.; Liu, C.-C.; Kim, C.; Lin, H.-C.; Chen, M.-C.; Chu, C.-W. Solution-Processed Small-Molecule Bulk Heterojunction Ambipolar Transistors. *Adv. Funct. Mater.* **2014**, *24*, 2057−2063.
(60) Briseno, A. L.; Mannsfeld, S. C. B.; Jenekhe, S. A.; Bao, Z.; Xia, Y. Introducing Organic Nanowire Transistors. *Mater. Today* **2008**, *11*, 38−47.
(61) Facchetti, A.; Mushrush, M.; Yoon, M.-H.; Hutchison, G. R.; Ratner, M. A.; Marks, T. J. Building Blocks for n-Type Molecular and Polymeric Electronics. Perfluoroalkyl- versus Alkyl-Functionalized Oligothiophenes (nT; n = 2−6). Systematics of Thin Film Microstructure, Semiconductor Performance, and Modeling of Majority Charge Injection in Field-Effect Transistors. *J. Am. Chem. Soc.* **2006**, *128*, 12851−12869.
(62) Yoon, M.-H.; Kim, C.; Facchetti, A.; Marks, T. J. Gate Dielectric Chemical Structure-Organic Field-Effect Transistor Performance Correlations for Electron, Hole, and Ambipolar Organic Semiconductors. *J. Am. Chem. Soc.* **2004**, *126*, 13859−13874.
(63) Yang, H.; Shin, T. J.; Ling, M.-M.; Cho, K.; Ryu, C. Y.; Bao, Z. Conducting AFM and 2D GIXD Studies on Pentacene Thin Films. *J. Am. Chem. Soc.* **2005**, *127*, 11542−11543.
(64) Tremel, K.; Fischer, F. S. U.; Kayunkid, N.; Di Pietro, R.; Tkachov, R.; Kiriy, A.; Neher, D.; Ludwigs, S.; Brinkmann, M. Charge Transport Anisotropy in Highly Oriented Thin Films of the Acceptor Polymer P(NDI2OD-T2). *Adv. Energy Mater.* **2014**, *4*, 1301659.
(65) Crossland, E. J. W.; Tremel, K.; Fischer, F.; Rahimi, K.; Reiter, G.; Steiner, U.; Ludwigs, S. Anisotropic Charge Transport in Spherulitic Poly(3-hexylthiophene) Films. *Adv. Mater.* **2012**, *24*, 839−844.
(66) Rivnay, J.; Jimison, L. H.; Northrup, J. E.; Toney, M. F.; Noriega, R.; Lu, S.; Marks, T. J.; Facchetti, A.; Salleo, A. Large Modulation of Carrier Transport by Grain-Boundary Molecular Packing and Microstructure in Organic Thin Films. *Nat. Mater.* **2009**, *8*, 952−958.

DOI: 10.1021/acsami.6b02788
ACS Appl. Mater. Interfaces 2016, 8, 14077−14087